frontiers | Frontiers in Radiology

TYPE Original Research
PUBLISHED 18 July 2025
DOI 10.3389/fradi.2025.1638294

OPEN ACCESS

EDITED BY
Dominic Gascho,
University of Zurich, Switzerland

REVIEWED BY
Sanjana Santhosh Kumar,
Eastmaninstitutet, Sweden
Akos Mikolicz,
Semmelweis University, Hungary

*CORRESPONDENCE
Anika Kofod Petersen
anko@forens.au.dk

RECEIVED 03 June 2025
ACCEPTED 30 June 2025
PUBLISHED 18 July 2025

CITATION
Kofod Petersen A, Villesen P and Staun Larsen L (2025) The oral fingerprint: rapid 3D comparison of palatal rugae for forensic identification.
Front. Radiol. 5:1638294.
doi: 10.3389/fradi.2025.1638294

The oral fingerprint: rapid 3D comparison of palatal rugae for forensic identification

Anika Kofod Petersen[1]*, Palle Villesen[2,3] and Line Staun Larsen[1,4]

[1]Department of Forensic Medicine, Aarhus University, Aarhus, Denmark, [2]Bioinformatics Research Centre, Aarhus University, Aarhus, Denmark, [3]Department of Clinical Medicine, Aarhus University, Aarhus, Denmark, [4]Department of Dentistry and Oral Health, Aarhus University, Aarhus, Denmark

Intoduction: The palatal rugae have been suggested to be just as unique as the human fingerprint. Therefore, endeavors have been made to utilize this uniqueness for the identification of disaster victims. With the rise of digital 3D dental data, computational comparisons of palatal rugae have become possible. But a direct comparison of the full palatal scan by iterative closest point (ICP) has shown to be tedious and demands a knowledge of superimposition software.
Methods: Here, we propose (1) an automatic extraction of the palatal rugae ridges from the 3D scans, followed by (2) ICP of the extracted ridges.
Results: Pairwise comparisons of palates take less than a second, and in this study, it was possible to distinguish between palates from the same individual vs. palates from different individuals with a receiver operating characteristic area-under-the-curve of 0.994.
Discussion: This shows that the extraction of the palatal rugae ridges is a potential efficient addition to the toolbox of a forensic odontologist for disaster victim identification.

KEYWORDS

palatal rugae, identification, automation, biometrics, forensic odontology

1 Introduction

In the case of disasters, forensic odontology is applied in the identification of the disaster victims as one of the primary identifiers, alongside DNA analysis and fingerprints (1–4). Forensic odontology holds an advantage in disaster victim identification since the dental structures are highly preserved in diverse disaster scenarios, including withstanding fires and decomposition (5, 6). Furthermore, in many countries, *ante mortem* data are often relatively easy to access in the form of clinical dental records, while for the other primary identifiers, *ante mortem* data can be limited or require laborious sampling. In forensic odontology, information gathered from dental records is compared with the victim's current dentition to get any insights into identification, i.e., any dental work, such as fillings or crowns, or any characteristic oral morphology (2–4, 7). For these traits to aid in the identification of the individual, the sum of traits must be unique enough for the forensic odontologist to make a confident decision (3).

The palatal rugae, the ridges at the roof of the mouth, have been hypothesized to construct just as unique a pattern as a fingerprint, and this is why this morphological structure is also considered for identification purposes (8–15). Even though this hypothesis has not been unanimously accepted, several studies point toward rugae uniqueness between individuals (8, 9, 11–13), even showing differences between monozygotic twins (14–17). Even though the palatal rugae do not withstand as diverse disaster scenarios as the dentition, the protected placement in the oral cavity could make it less sensitive to disaster settings than fingerprints.

This uniqueness has triggered endeavors to utilize the 3D landscape of palatal rugae for identification (8–10, 13, 17). Specifically, with the rise of 3D intraoral scanners (18–21), the palatal rugae can be scanned and represented as a 3D mesh. Several researchers have investigated different ways to compare 3D scans of palatal rugae, to aid in identification (8–10, 13, 16, 17, 22–27). Most of these studies cover superimposition methods (8, 10, 16, 17, 21, 22, 24–26), many being versions of the iterative closest point (ICP) algorithm (8, 10, 16, 17, 21, 22, 24, 26), where the distances between one 3D mesh is minimized to the other to create a "best-fit" overlay to then evaluate goodness of fit. When considering palatal rugae comparison, ICP has two major drawbacks (19, 28, 29). First, it is sensitive to the cropping of the palatal rugae (28, 29). If the tooth-gingiva border is meticulously traced when cutting out the rugae from an intraoral 3D scan, there is a risk of ICP optimizing the fit of the dental traces, meaning the main driver for a good overlay may be tooth positions. This is not necessarily unwanted behavior, but in these cases, no guarantee can be made that the matching of the palatal rugae is what is being investigated. The rugae surfaces to be compared would be highly affected by the cropping method of the surface. If the surfaces are manually cropped, such subjectivity could affect the ICP comparison to such an extent that different forensic investigators would find different best matching identities (28). Other studies localize the palatal rugae ridges by manually tracing the ridges, which once again, adds subjectivity to the identification process, which is highly undesirable (24). To truly guarantee that all individuals are treated equally in the context of disaster victim identification, subjectivity must be eliminated from the entire palatal rugae matching process, i.e., by automation. The other drawback of ICP is time, since ICP is an all-to-all comparison and a 3D scan typically harbors hundreds of thousands of data points (8, 17, 28, 29).

Even though superimposition techniques show good results, reaching an optimal overlay between two high-resolution 3D surfaces is so time-consuming that it is difficult to apply in many scenarios (8, 17), for example, when considering a disaster victim identification case, where one 3D mesh of a palatal rugae surface is compared with a whole database of *ante mortem* 3D meshes. This process is then iterated for every victim of the disaster. Therefore, even though good results have been shown previously, there is a need for optimizing the superimposition method to make it feasible for palatal rugae comparison in forensic odontology disaster victim identification (8, 17).

One way is to not optimize the superimposition methods directly but instead preprocess the 3D scans to reduce the number of data points and only focus the process on the palatal rugae and not the rest of the palatal tissue. It has been suggested by Zhao et al. to manually extract the palatal rugae prior to ICP (24), but since this is both-time consuming and adds subjectivity in the data extraction step, an automated approach should be preferred. This study investigates the feasibility of automated extraction of the palatal rugae prior to ICP. This eliminates the problems associated with manual extraction of the palatal rugae, while it retains the lower processing time and the unique traits of the palatal rugae (8, 17, 24).

2 Materials and methods

The palatal surface was manually cut (avoiding tracing the dentition border) from 102 intraoral scans of 51 healthy volunteering individuals (ranging from 23 to 61 years of age), from a dataset previously presented by Kofod Petersen and colleagues (30). Each individual was subject to two intraoral scans approximately 6 months apart (30). Each scan was saved as a 3D surface mesh file in stl format (30). The same scanner, a Primescan AC Sirona Dental Systems GmbH intraoral dental scanner, was used for all scans.

All computations in this study were performed on a machine with an 11th Gen Intel Core i7-1165G7, 2.80 GHz (x86_64) processor and 8GB RAM, thus matching a laptop device. All code was written in Python 3.10 with the use of the Trimesh library (31) for rugae extraction and the Open3D library (32) for ICP registration. An illustration of the workflow can be seen in Figure 1.

To extract the palatal rugae from the intraoral scans, the scans were initially decimated using quadratic decimation to 50% resolution (31). Afterward, the discrete mean curvature measurements were extracted from the surface mesh and the curvatures were normalized (31). The normalized curvature measures were then used to find the rugae ridges as follows. First, the 5% lowest curvatures, i.e., "the valleys," were extracted to ensure that the border between the rugae ridge and the flat palatal soft tissue was included in the analysis. Then, the 30%, 25%, 20%, 15%, 10%, and 5% highest curvatures, i.e., "the hills," were extracted as point clouds. This means that each intraoral scan generated six files. This was done to investigate how much of the rugae ridges was needed for proper superimposition.

When reporting a similarity score, the score represents how well a pair of meshes aligns with one another. Having 51 individuals with 2 scans ensures that there are 51 matching pairs. To avoid biasing the reported performance, the dataset was randomly split into a validation set and a testing set. The validation set consisted of 26 of the matching pairs and 650 mismatching pairs (26×25). The testing dataset consisted of the remaining 25 matching pairs and 600 mismatching pairs (25×24).

Pairs of rugae 3D meshes were compared using ICP registration with 1,000 maximum iterations and a maximum correspondence distance of 3 mm (32). This resulted in inlier root mean squared error (RMSE) measures for each comparison, describing the quality of alignment of the rugae meshes. A low inlier RMSE equals a good alignment. First, the inlier RMSE of all the matching pairs was compared with the inlier RMSE of the mismatching pairs of the validation dataset. To decide how much of the palatal rugae curvature to include in the final methodology, different amounts of curvatures were tested on the validation data, and the optimal amount of curvature was decided upon, by evaluating which amount of curvature showed the greatest difference between the matching and the mismatching distribution. The amount of curvature that showed the highest Wasserstein distance between matching and mismatching pair inlier RMSE was chosen. This is later reflected in Figure 2. If the method performs well, the matching pairs will have a low inlier RMSE, while the mismatching pairs will have a high inlier RMSE.

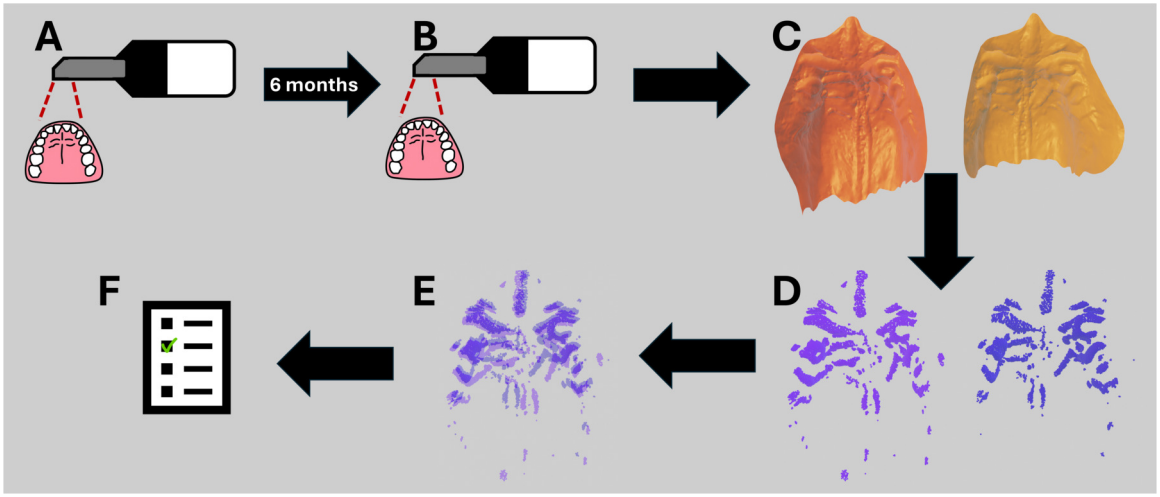

FIGURE 1
Workflow from data acquisition with the intraoral scanner to the resulting comparison inlier RMSE. **(A)** First intraoral scan of the healthy volunteers. **(B)** Second intraoral scan of the healthy volunteers after 6 months. **(C)** Isolation of the mesh palate from the intraoral scans. **(D)** Extraction of rugae ridges. **(E)** ICP registration of the extracted rugae ridges. **(F)** Inlier RMSE score of the ICP registrations, scoring how well the extracted rugae ridges match.

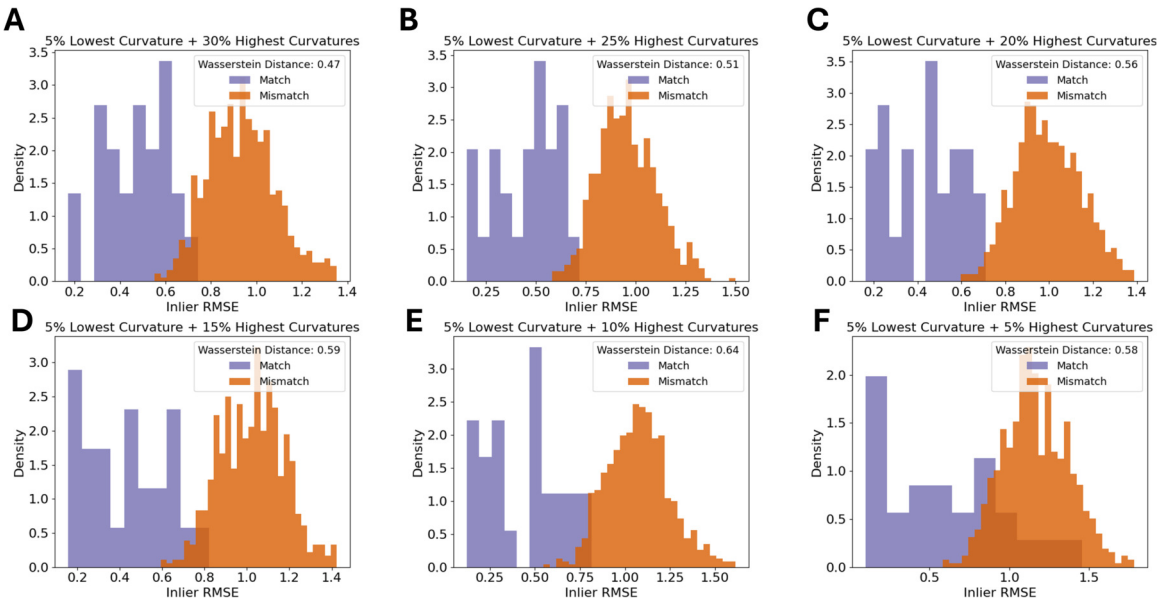

FIGURE 2
Density histograms of inlier RMSE of matching pairs and mismatching pairs for a decreasing amount of palatal curvature data. The figure shows the 5% lowest curvatures and the **(A)** 30% highest curvatures, **(B)** 25% highest curvatures, **(C)** 20% highest curvatures, **(D)** 15% highest curvatures, **(E)** 10% highest curvatures, and **(F)** 5% highest curvatures.

To report how well the method is at scoring the pairs appropriately, and to obtain an estimate of robustness of the procedure, we used a repeated sampling procedure (similar to bootstrapping) on the test set. For 1,000 iterations, all matching pairs and 200 randomly selected mismatching pairs from the test dataset were compared. The relation between the true-positive rate and the false-positive rate was investigated using receiver operating characteristic (ROC) area-under-the-curve (AUC).

3 Results

3.1 Defining the model using the validation set

The first step was to find an appropriate amount of rugae curvatures to include in a comparison. As seen in Figure 2, the largest distance between the matching and the mismatching inlier

TABLE 1 Lowest 6 inlier RMSE scores for each query rugae in the validation dataset.

Rank 1	Rank 2	Rank 3	Rank 4	Rank 5	Rank 6
0.305*	0.638	0.878	0.918	0.924	0.931
0.216*	0.733	0.779	0.789	0.837	0.877
0.606*	0.949	0.964	1.028	1.035	1.053
0.687*	0.872	1.038	1.125	1.127	1.137
0.685	**0.778***	0.836	0.98	0.991	0.992
0.529*	0.751	0.791	0.819	0.833	0.842
0.640*	1.038	1.106	1.106	1.111	1.118
0.659*	0.833	1.067	1.069	1.094	1.094
0.394*	0.636	0.790	0.798	0.802	0.813
0.816*	0.919	1.054	1.134	1.169	1.197
0.122*	0.649	0.807	0.816	0.819	0.820
0.296*	0.796	0.834	0.855	0.871	0.898
0.265*	0.725	0.741	0.76	0.763	0.798
0.142*	0.739	0.803	0.809	0.826	0.826
0.221*	0.803	0.833	0.843	0.898	0.911
0.687	**0.689***	0.707	0.775	0.779	0.832
0.188*	0.546	0.745	0.8	0.804	0.856
0.486*	0.938	0.961	0.998	1.008	1.067
0.571*	0.845	0.896	0.986	1.020	1.070
0.508*	0.825	0.877	0.895	0.948	0.975
0.478*	0.802	0.881	0.884	0.918	0.921
0.224*	0.964	1.034	1.041	1.052	1.056
0.497*	0.875	0.877	0.916	0.921	0.942
0.294*	0.763	0.785	0.862	0.877	0.897
0.536*	0.891	0.922	0.958	0.986	1.005
0.169*	0.758	0.829	0.829	0.838	0.858

True match indicated with bold and asterisk.

TABLE 2 Lowest 6 inlier RMSE scores for each query rugae in the test dataset.

Rank 1	Rank 2	Rank 3	Rank 4	Rank 5	Rank 6
0.536*	0.707	0.725	0.768	0.826	0.829
0.849*	0.927	0.952	0.955	0.966	0.978
0.681*	0.823	0.852	0.882	0.889	0.954
1.091	1.112	1.209	1.234	1.285	**1.291***
0.273*	0.84	0.843	0.854	0.961	0.984
0.253*	0.662	0.685	0.787	0.792	0.857
0.852*	1.083	1.083	1.102	1.146	1.158
0.356*	0.733	0.887	0.894	0.907	0.911
0.294*	0.983	1.015	1.049	1.06	1.063
0.534*	0.855	0.861	0.864	0.868	0.878
0.595*	0.845	0.966	0.982	0.992	0.999
0.674*	0.91	0.977	0.978	1.031	1.068
0.761*	0.787	0.822	0.837	0.861	0.903
0.499*	0.757	0.772	0.793	0.811	0.818
0.548*	0.725	0.75	0.805	0.827	0.868
0.155*	0.784	0.794	0.85	0.854	0.854
0.449*	0.828	0.836	0.889	0.919	0.959
0.403*	0.86	0.953	1.012	1.023	1.053
0.495*	0.802	0.861	0.92	0.939	0.94
0.613*	0.726	0.75	0.781	0.817	0.825
0.712*	1.031	1.053	1.061	1.066	1.109
0.853*	0.882	0.976	1.002	1.012	1.152
0.415*	0.648	0.675	0.731	0.759	0.776
0.127*	0.784	0.804	0.832	0.853	0.872
0.324*	0.723	0.816	0.818	0.87	0.891

True match indicated with bold and asterisk.

RMSE distributions was found when using the 5% lowest curvatures and the 10% highest curvatures.

When using 10% of the highest curvatures to calculate inlier RMSE, nearly all of the 26 rugae had the lowest inlier RMSE with the correct match (Table 1). In two cases, the correct rugae were ranked as number 2. In these two cases, the difference in the similarity score between the outranking mismatch and the match was 0.094 and 0.001, respectively, as seen in Table 1. In cases where the match is the best-ranking comparison, there was a mean difference between rank 1 and rank 2 of 0.393, indicating that a great difference between the best-ranking and second-best-ranking comparison is a good indicator of confidence.

3.2 Testing the scoring

The inlier RMSE scoring was tested on the test data with palatal rugae from the 10% highest curvatures (and the 5% lowest curvatures) on the remaining 25 palatal meshes. Following the same procedure as for the validation dataset, we saw that 24/25 of the matches were found to have the lowest inlier RMSE (Table 2). The single false-negative had the correct match ranked 6, but with an overall high RMSE.

We found the scoring procedure to have an extremely high performance with a mean ROC-AUC of 0.994 (Figure 2). The 1,000 random subsamples also showed the procedure to be extremely robust, with AUCs ranging from 0.988 to 0.998 (Figure 3, shaded band).

3.3 Processing time

Extracting the palatal curvatures and saving the rugae files are only done once per intraoral scan and can easily be done in parallel. Therefore, this part of comparison is not expected to be time limiting. In contrast, since ICP is done for all victims across all *ante mortem* 3D meshes, the number of ICP comparisons will significantly increase with the number of victims and the size of the *ante mortem* database.

On a machine with an 11th Gen Intel Core i7–1165G7, 2.80 GHz (x86_64) processor and 8GB RAM, a comparison of one pair of extracted rugae curvatures took on average 0.078 s (PI 95% from 0.011 to 0.251 s). To perform the same analysis on full palatal rugae scans took on average 47.9 s (PI 95% from 8.24 to 157.27 s). These tendencies are depictured in Figure 4.

For exemplification, 500 comparisons were made where 51 were matches and the remaining 449 were mismatches. To perform ICP on only the 500 extracted rugae comparisons took a total of 43 s, while ICP on the 500 full palatal comparisons took a total of 6 h 39 min and 34 s. Despite the higher amount of data, the performance was worse when using the full palatal meshes (Figure 5). It seems that the extra surface information and the difference in mesh border might drive the ICP alignment

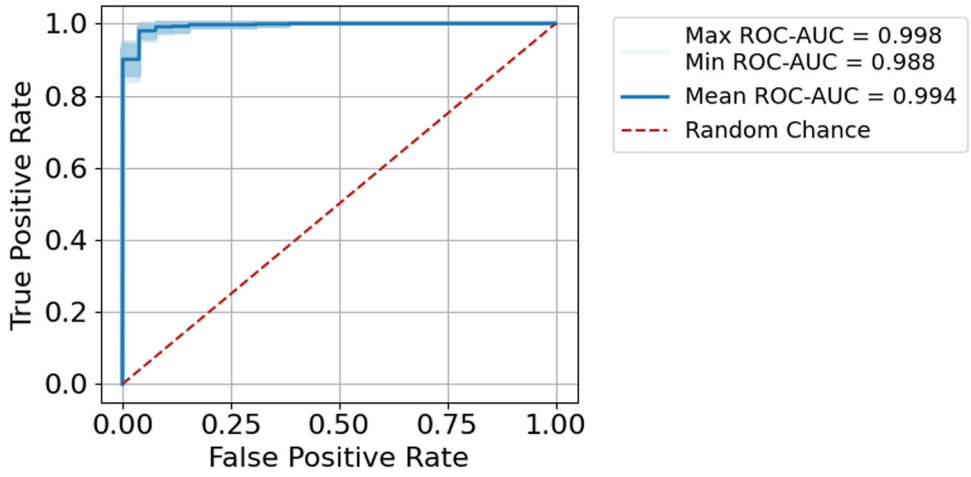

FIGURE 3
ROC-AUC for the test data using 1,000 iterations of subsampling.

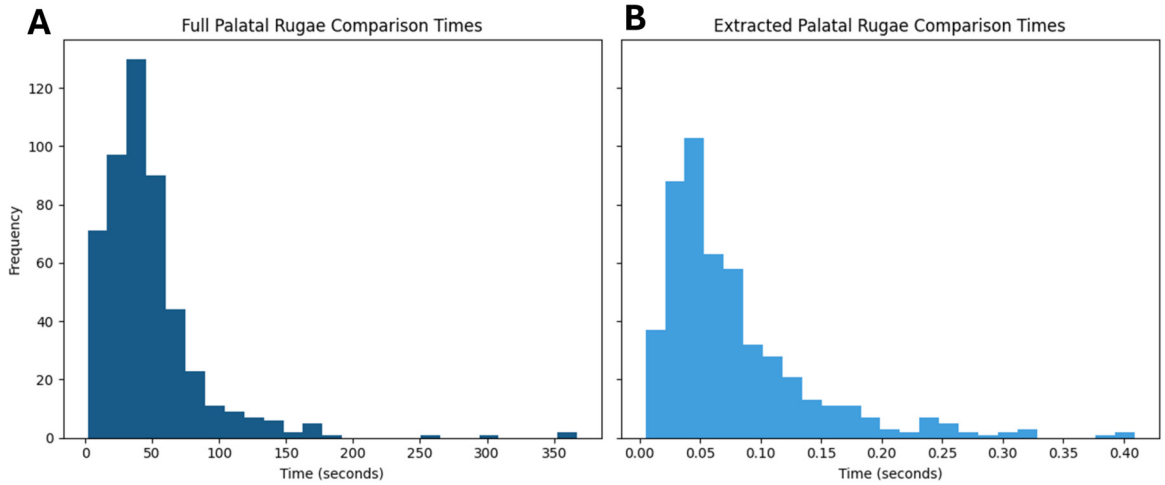

FIGURE 4
Histograms of comparison times for (A) full palatal rugae and (B) extracted palatal rugae. Panel (A) and (B) shares y-axis.

away from the optimal rugae alignment, making automatic ICP registration of full palatal meshes difficult, resulting in poor performance (19, 29, 30).

4 Discussion

For disaster victim identification using Forensic Odontology, an automated workflow for palatal rugae comparison in 3D could be beneficial (8–10, 17, 18, 23–27). But with the preferred methodology (ICP) being too slow when it comes to comparing full palatal meshes, this is currently not feasible for major disasters (8, 17).

However, by automatically extracting the 10% highest curvatures and the 5% lowest curvatures from the palatal rugae scans, a comparison can be done in less than a second, which is no longer a bottle neck when it comes to disaster victim identification. This data preprocessing step increases the speed of comparisons by magnitudes, alleviating the time constraint.

Furthermore, the extraction of rugae curvatures ensures that the optimal alignment is focused on the rugae ridges and no other features of the palatal surface, such as cropping border and tooth position.

The higher level of detail in the full palatal meshes does not increase separability between matches and mismatches. Rather the contrary, as seen when comparing Figures 2, 5. We see an increase in speed and separation when using only the extracted palatal curvatures, highly advocating for the use of extracted palatal rugae instead of full palatal meshes.

To utilize rugae uniqueness for identification purposes, there is a need for preserved rugae patterns. This means that in disaster victim identification scenarios where the palatal soft tissue has suffered great damage, e.g., by heat or decomposition, this rugae

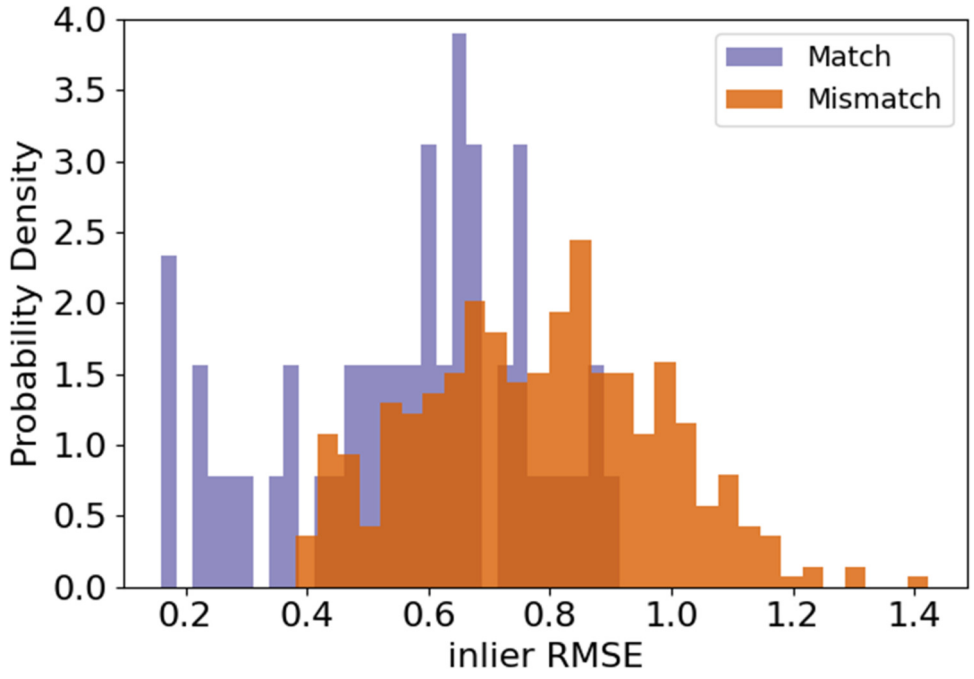

FIGURE 5
Inlier RMSE after ICP on full palatal rugae for matches and mismatches.

comparison methodology would not be feasible. But if the palatal rugae are intact, they can serve as an addition to other identification methods, like dental comparison, DNA, and fingerprints, now without being a time-limiting step.

The acquisition of the palatal rugae can be considered a limitation of this study. With a time difference of 6 months between the first and the second acquisition, the palatal rugae are not expected to have changed much throughout this study. Although it is hypothesized that the changes to the palatal rugae through an individual's life is limited (15), it is still expected that traumatic events, such as scarring, could make changes to the rugae ridges. Also, orthodontic treatment might change the surface structures of the palate, but to what extent is still to be investigated. Such changes to the palatal rugae are not covered by the short time difference applied in this study.

The fact that the same scanner was used for both acquisitions limits the systematic variability in this study. It is expected to observe a certain degree of systematic variability when using different scanners (33), as would be the case in a real-life disaster victim identification scenario. It is suggested that the variation between scans of the palate is less than what is observed for the variation of the dentition surface when using some scanners (14), and that the systematic variation between scanners is decreasing as scanners get better, and might not pose clinical relevance, especially in the future.

The major difference between this study and previous studies about rugae superimposition is the data preprocessing steps used (8, 10, 16, 22, 24–26). This study automatically extracts the rugae ridges, while other studies either compared the entire palate (8, 10, 16, 26), used manually set landmarks to define a region of interest (22), or manually cut out the rugae ridges (24). Manual landmarks and manual extraction are affected by subjectivity and is therefore not a suitable method for data preprocessing in a forensic context. Figures 4, 5 serve as benchmarking between the comparison of a full palate and the suggested extraction method, showing the benefit of automatic rugae extraction.

For future integration into the forensic toolbox, the extraction of the palatal rugae might serve as an initial data preprocessing step, making the palatal data easily digestible for machine learning models. It is plausible that better rugae comparison algorithms than ICP would be developed in the future, and that the automatic rugae ridge extraction could serve as a feature reduction step toward better palate matching.

This study shows that automatic extraction of palatal rugae from 3D intraoral scans can be used in combination with ICP for disaster victim identification, without causing a major bottleneck due to processing time (8–10, 16, 17, 22–27). The inlier RMSE of the extracted palatal rugae can serve as a similarity score, used for ranking possible matches. The ranking of the palatal rugae comparison can then be used in addition to other forensic odontological techniques for the forensic odontologist to identify disaster victims (3).

Data availability statement

The datasets presented in this article are not readily available because this study includes data that can be considered personal dental data, which the authors are not authorized to share.

Requests to access the datasets should be directed to Anika Kofod Petersen, anko@forens.au.dk.

Ethics statement

The studies involving humans were approved by exception from notification by the Danish National Committee on Health Research Ethics (NVK). The studies were conducted in accordance with the local legislation and institutional requirements. The participants provided their written informed consent to participate in this study.

Author contributions

AK: Validation, Conceptualization, Formal analysis, Visualization, Methodology, Writing – review & editing, Writing – original draft, Investigation, Project administration, Data curation. PV: Writing – review & editing, Supervision, Project administration, Conceptualization. LS: Writing – review & editing, Project administration, Funding acquisition, Conceptualization, Supervision.

Funding

The author(s) declare that financial support was received for the research and/or publication of this article. This study was funded by AUFF NOVA (Grant number: AUFF-E-2021-9-14).

Acknowledgments

We thank Professor Emerita, Dorthe Arenholt Bindslev, for her valuable discussions and insightful input during the conceptualization phase of this work.

Conflict of interest

The authors declare that the research was conducted in the absence of any commercial or financial relationships that could be construed as a potential conflict of interest.

Generative AI statement

The author(s) declare that no Generative AI was used in the creation of this manuscript.

Publisher's note

References

1. Interpol. Disaster Victim Identification (DVI). (2025). Available online at: https://www.interpol.int/en/How-we-work/Forensics/Disaster-Victim-Identification-DVI (Accessed February 19, 2025).

2. Berketa JW, James H, Lake AW. Forensic odontology involvement in disaster victim identification. *Forensic Sci Med Pathol.* (2012) 8(2):148–56. doi: 10.1007/s12024-011-9279-9

3. Interpol. Interpol Disaster Victim Identification Guide. Part B, Annexure 8. Methods of Identification (2023).

4. Sweet D. INTERPOL DVI best-practice standards—an overview. *Forensic Sci Int.* (2010) 201(1):18–21. doi: 10.1016/j.forsciint.2010.02.031

5. de Boer HH, Roberts J, Delabarde T, Mundorff AZ, Blau S. Disaster victim identification operations with fragmented, burnt, or commingled remains: experience-based recommendations. *Forensic Sci Res.* (2020) 5(3):191–201. doi: 10.1080/20961790.2020.1751385

6. Hill AJ, Lain R, Hewson I. Preservation of dental evidence following exposure to high temperatures. *Forensic Sci Int.* (2011) 205(1):40–3. doi: 10.1016/j.forsciint.2010.08.011

7. Kvaal SI. Collection of post mortem data: DVI protocols and quality assurance. *Forensic Sci Int.* (2006) 159:S12–4. doi: 10.1016/j.forsciint.2006.02.003

8. Bjelopavlovic M, Degering D, Lehmann KM, Thiem DGE, Hardt J, Petrowski K. Forensic identification: dental scan data sets of the palatal fold pairs as an individual feature in a longitudinal cohort study. *Int J Environ Res Public Health.* (2023) 20(3):2961. doi: 10.3390/ijerph20032691

9. Zhang X, Luo Q, Shangguan H, Wu Y, Li B, Yang J. Three-dimensional palatal rugae recognition based on cyclic spectral analysis. *Biomed Signal Process Control.* (2021) 68:102718. doi: 10.1016/j.bspc.2021.102718

10. Choi DS, Jeong YM, Jang I, Jost-Brinkmann PG, Cha BK. Accuracy and reliability of palatal superimposition of three-dimensional digital models. *Angle Orthod.* (2010) 80(4):497–503. doi: 10.2319/101309-569.1

11. Chong JA, Syed Mohamed AMF, Marizan Nor M, Pau A. The heritability of palatal rugae morphology among siblings. *J Forensic Sci.* (2020) 65(6):2000–7. doi: 10.1111/1556-4029.14507

12. Gupta AA, Kheur S, Alshehri A, Awadh W, Ahmed ZH, Feroz SMA, et al. Is palatal rugae pattern a reliable tool for personal identification following orthodontic treatment? A systematic review and meta-analysis. *Diagnostics (Basel).* (2022) 12(2):418. doi: 10.3390/diagnostics12020418

13. Roselli L, Mele F, Suriano C, Santoro V, Catanesi R, Petruzzi M. Palatal rugae assessment using plaster model and dental scan: a cross-sectional comparative analysis. *Front Oral Health.* (2024) 5:1456377. doi: 10.3389/froh.2024.1456377

14. Mikolicz Á, Simon B, Lőrincz G, Vág J. Clinical precision of Aoralscan 3 and Emerald S on the palatal and dentition areas: evaluation for forensic applications. *J Dent.* (2025) 153:105455. doi: 10.1016/j.jdent.2024.105455

15. Mikolicz A, Simon B, Gáspár O, Shahbazi A, Vag J. Reproducibility of the digital palate in forensic investigations: a two-year retrospective cohort study on twins. *J Dent.* (2023) 135:104562. doi: 10.1016/j.jdent.2023.104562

16. Taneva E, Evans C, Viana G. 3D Evaluation of palatal rugae in identical twins. *Case Rep Dent.* (2017) 2017:2648312. doi: 10.1155/2017/2648312

17. Simon B, Aschheim K, Vág J. The discriminative potential of palatal geometric analysis for sex discrimination and human identification. *J Forensic Sci.* (2022) 67(6):2334–42. doi: 10.1111/1556-4029.15110

18. Hidemichi K, Wataru H, Futoshi K, Kyoko T, Toshiyuki T, Jun Y, et al. Accuracy and practicality of intraoral scanner in dentistry: a literature review. *J Prosthodont Res.* (2020) 64(2):109–13. doi: 10.1016/j.jpor.2019.07.010

19. Perkins H, Chiam TL, Forrest A, Higgins D. 3D Dental images in forensic odontology: a scoping review of superimposition approaches utilizing 3D imaging. *Forensic Imaging.* (2025) 40:200622. doi: 10.1016/j.fri.2024.200622

20. Perkins H, Hughes T, Forrest A, Higgins D. 3D dental records in Australian dental practice—a hidden gold mine for forensic identification. *Aust J Forensic Sci.* (2024) 57(3):322–39. doi: 10.1080/00450618.2024.2359432

21. Mourouzis P. Critical methodological factors influencing the accuracy of intraoral scanners in digital dentistry research. *Comput Biol Med*. (2025) 187:109780. doi: 10.1016/j.compbiomed.2025.109780

22. Garib D, Miranda F, Yatabe MS, Lauris JRP, Massaro C, McNamara JA Jr., et al. Superimposition of maxillary digital models using the palatal rugae: does ageing affect the reliability? *Orthod Craniofac Res*. (2019) 22(3):183–93. doi: 10.1111/ocr.12309

23. Shangguan H, Yang T, Luo Q, Zhang X, Li B, Wang S. 3D palatal rugae recognition based on fractional Fourier transform. *Digit Signal Process*. (2023) 133:103873. doi: 10.1016/j.dsp.2022.103873

24. Zhao J, Du S, Liu Y, Saif BS, Hou Y, Guo YC. Evaluation of the stability of the palatal rugae using the three-dimensional superimposition technique following orthodontic treatment. *J Dent*. (2022) 119:104055. doi: 10.1016/j.jdent.2022.104055

25. Farronato M, Begnoni G, Boodt L, Thevissen P, Willems G, Cadenas de Llano-Pérula M. Are palatal rugae reliable markers for 3D superimposition and forensic human identification after palatal expansion? A systematic review. *Forensic Sci Int*. (2023) 351:111814. doi: 10.1016/j.forsciint.2023.111814

26. Gibelli D, De Angelis D, Pucciarelli V, Riboli F, Ferrario VF, Dolci C, et al. Application of 3D models of palatal rugae to personal identification: hints at identification from 3D-3D superimposition techniques. *Int J Legal Med*. (2018) 132(4):1241–5. doi: 10.1007/s00414-017-1744-x

27. Santhosh Kumar S, Chacko R, Kaur A, Ibrahim G, Ye D. A systematic review of the use of intraoral scanning for human identification based on palatal morphology. *Diagnostics (Basel)*. (2024) 14(5):531. doi: 10.3390/diagnostics14050531

28. Besl PJ, McKay ND. A method for registration of 3-D shapes. *IEEE Trans Pattern Anal Mach Intell*. (1992) 14(2):239–56. doi: 10.1109/34.121791

29. Rusinkiewicz S, Levoy M. Efficient variants of the ICP algorithm. *Proceedings Third International Conference on 3-D Digital Imaging and Modeling* (2001). p. 145–52.

30. Kofod Petersen A, Arenholt Bindslev D, Forgie A, Villesen P, Staun Larsen L. Objective comparison of 3D dental scans in forensic odontology identification. *medRxiv (preprint)*. (2025):2025.03.31.25324929.

31. Dawson-Haggerty M. Trimesh. (2019). Available online at: https://trimesh.org/ (Accessed January 05, 2023).

32. Zhou Q-Y, Park J, Koltun V. Open3D: A Modern Library for 3D Data Processing. *arXiv*. (2018):180109847.

33. Ye J, Wang S, Wang Z, Liu Y, Sun Y, Ye H, et al. Comparison of the dimensional and morphological accuracy of three-dimensional digital dental casts digitized using different methods. *Odontology*. (2023) 111(1):165–71. doi: 10.1007/s10266-022-00736-2